JOURNAL OF GEOPHYSICAL RESEARCH, VOL. 112, F01002, doi:10.1029/2006JF000474, 2007

Development and response of a coupled catchment fan system under changing tectonic and climatic forcing

Alexander L. Densmore,[1] Philip A. Allen,[1,2] and Guy Simpson[1]

Received 30 January 2006; accepted 8 September 2006; published 1 February 2007.

[1] Sediment fans are a potentially useful and underexploited recorder of Earth's climatic and tectonic history, but historical observations have led to conflicting views on the importance of tectonic, climatic, and lithologic variables in controlling fan morphology and deposition. A one-dimensional model of a sediment fan and its associated catchment is used to explore the sensitivity of such simple sediment routing systems to perturbations in fault slip and precipitation rates. A transport-limited catchment is coupled to a fan whose surface slope is set by the balance between catchment sediment efflux and the available tectonically generated basin accommodation. Rock uplift rate is spatially variable across the model space. Increasing the fault slip rate, or decreasing the precipitation rate, leads to an increase in fan slope, temporary back-stepping of the fan toe, and a pronounced angular unconformity. Conversely, a decrease in slip rate, or an increase in precipitation rate, results in a decrease in fan slope, and progradation and eventual stabilization of the fan toe. Once perturbed, the system evolves toward a new equilibrium state with time constants of ~0.5 to 2 Myr; these response times are insensitive to slip rate but are strongly dependent on precipitation rate. Variations in fan slope are well described by a dimensionless parameter that expresses equilibrium slope as a function of slip rate, precipitation rate, system size, and catchment lithology. This parameter holds promise as a predictive tool in inverting the morphology of natural fans for environmental variables.

Citation: Densmore, A. L., P. A. Allen, and G. Simpson (2007), Development and response of a coupled catchment fan system under changing tectonic and climatic forcing, *J. Geophys. Res.*, *112*, F01002, doi:10.1029/2006JF000474.

1. Introduction

[2] The Earth's surface is a dynamic interface that, at its most basic level, routes sediment from sources to sinks. To grasp how this surface evolves, we must first understand how sediment routing systems respond to perturbations in their tectonic and climatic driving forces. The timescales over which this response occurs are vital for understanding the fidelity with which landscapes, or the sedimentary products that are routed through them, can record the tectonic or climatic history of a region [e.g., *Humphrey and Heller*, 1995; *Métivier and Gaudemer*, 1999; *Castelltort and van den Driessche*, 2003]. Put another way, are landscapes and their associated sedimentary records "reactive" or "buffered" [*Allen*, 2007], particularly in the face of high-frequency forcing variations? This clearly determines whether it is safe to invert the stratigraphic record or the morphometric properties of a landscape to reveal information on driving mechanisms.

[3] Recent work on landscape response has focused largely on specific elements in sediment routing systems, such as hillslopes [*Fernandes and Dietrich*, 1997], bedrock rivers in upland areas [e.g., *Whipple and Tucker*, 1999; *Whipple*, 2001; *Carretier and Lucazeau*, 2005], or alluvial river systems [e.g., *Paola et al.*, 1992; *Dade and Friend*, 1998; *Métivier et al.*, 1999; *Métivier and Gaudemer*, 1999; *Castelltort and van den Driessche*, 2003]. These studies risk overlooking the potential coupling and feedbacks between different landforms and processes within a sediment routing system [*Humphrey and Heller*, 1995]. The entire system may respond in different ways and over different scales, depending on the nature and frequency of the perturbation. *Allen* [2005] consequently likened the response of landscapes to the different frequencies produced by playing of a guitar chord, with different finger positions on different frets.

[4] We focus here on the behavior of one of the smallest and simplest complete sediment routing systems: an upland catchment where sediment is produced, and an adjacent fan where some or all of that sediment is deposited (Figure 1). Most catchment fan systems are limited in spatial scale and are amenable to a mass or volume balance since they are essentially closed in their sediment budget [*Whipple and Trayler*, 1996; *Allen and Densmore*, 2000]. They are ubiquitous features of tectonically active environments where rock uplift and accommodation generation are controlled by deformation on discrete upper crustal structures, including rifts, extensional fault blocks, strike-slip zones, and fold

[1]Institute of Geology, Department of Earth Sciences, ETH Zürich, Zürich, Switzerland.
[2]Now at Department of Earth Science and Engineering, Imperial College London, London, UK.

0148-0227/07/2006JF000474$09.00

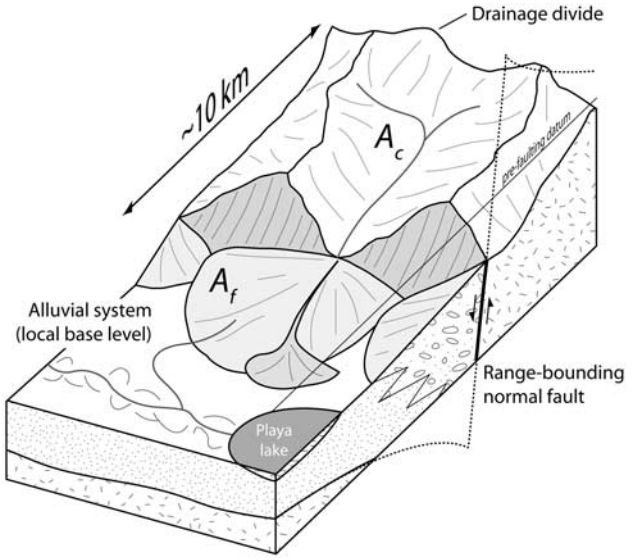

Figure 1. Schematic view of a typical catchment fan system. Upland block is separated from adjacent basin by an active crustal-scale fault. Catchment area A_c is typically related to fan area A_f through a power law relationship (equation (1)). Fan toe position is controlled by fan surface slope and local base level at the fan toe, which in this case is an axial alluvial system. Heavy solid line shows range-bounding fault; dotted line shows schematic across-strike displacement pattern.

thrust belts. As such, they form the basic building blocks of larger, more complex sediment routing systems.

[5] A key question is whether catchment fan systems are sensitive recorders of the tectonic and climatic histories of a region, and whether these different driving mechanisms can be recognized and separated from each other. Whereas much effort in resolving this question has focused on catchment form, particularly river long profiles [e.g., *Whipple and Tucker*, 1999; *Snyder et al.*, 2000; *Whipple and Tucker*, 2002; *van der Beek and Bishop*, 2003; *Wobus et al.*, 2006], considerably less recent attention has been paid to the associated depositional fans. Fans have the advantage of preserving the history of catchment sediment efflux and accommodation generation in their stratigraphy and in their plan view and cross-sectional geometry [e.g., *Fraser and DeCelles*, 1992]. In addition, we can build on a large body of basic observations of fan form and sedimentary characteristics in different geologic settings [*Bull*, 1962, 1964; *Denny*, 1965; *Hooke*, 1967, 1968; *Hooke and Rohrer*, 1977; *Whipple and Dunne*, 1992; *Gordon and Heller*, 1993; *Blair and McPherson*, 1994; *Blair*, 1999a, 1999b]. Pioneering work on the coupling between catchments and fans was carried out by *Humphrey and Heller* [1995], who presented a simple model of a mountain catchment and adjoining fan, each obeying different geomorphic rules and linked at the fan apex. They showed that perturbation of even this highly stylized model yielded complex, cyclic patterns of erosion and sedimentation, but did not extend their analysis to long-term landform development. *Pelletier* [2004] and *Carretier and Lucazeau* [2005] used similar models to argue that the presence of a downstream fan plays a key role in modulating river incision and long profile development, but did not consider the variations in, or the controls on, fan morphology.

[6] Starting from a set of basic observations on catchments and fans, we build a dynamical model of a single catchment fan system. Our objective is to use the simplest possible model that allows us to understand the response of the integrated system to changes in forcing mechanisms. We apply both tectonic and climatic perturbations to the system and focus on the response of geological or geomorphological variables that can be easily observed, such as fan slopes and lengths from head to toe. Our analysis clarifies some of the hitherto confusing correlations between tectonic and climatic boundary conditions, catchment sediment efflux, and fan slope and geometry, and identifies some key landscape-scale response times of the system.

2. Observations of Fan Geometry in Coupled Catchment Fan Systems

[7] The depositional fans of California and Nevada in the western United States were the subject of pioneering work during the middle part of the twentieth century [*Bull*, 1962, 1964; *Denny*, 1965; *Hooke*, 1967, 1968]. These studies provide a number of important, and to some extent forgotten, observations that must constrain any modeling of catchment fan systems in tectonically active regions. They also provide at least a qualitative idea of the fidelity of alluvial fans as recorders of tectonic and climatic variations through time. Here we summarize some of the key points that are relevant to our model experiments and predictions.

2.1. Fan Area and Length

[8] A number of workers have discussed the controls on fan area, motivated in part by a commonly observed power law relationship between fan area A_f and catchment area A_c [e.g., *Bull*, 1964; *Denny*, 1965; *Hooke*, 1968; *Whipple and Trayler*, 1996; *Allen and Hovius*, 1998]:

$$A_f = cA_c^n \tag{1}$$

where c and n are empirical coefficients and n is close to unity. *Bull* [1964] argued that fan areas in the San Joaquin Valley, California, were dependent largely on the erodibility of rocks in the catchment. Catchments underlain by weak rocks produce larger fans, presumably due to higher rates of long-term sediment supply, than those dominated by less erodible lithologies such as sandstone. *Whipple and Trayler* [1996] questioned this interpretation, pointing out that, counterintuitively, the catchments underlain by weak rocks are also significantly steeper than those in stronger rocks, which raises the possibility that differential rock uplift rates may play a role. *Hooke and Rohrer* [1977] demonstrated that, while differences in catchment erodibility produce second-order variations in fan areas in Death Valley, fault slip rates are the dominant controlling factor. Likewise, *Whipple and Trayler* [1996] and *Allen and Hovius* [1998] argued, largely on theoretical grounds, that fault slip rate must be the dominant control on fan area, but left the question of how this occurs somewhat open. High rock uplift rates in the catchment will promote high sediment supply and thus large fans, with long radial lengths from

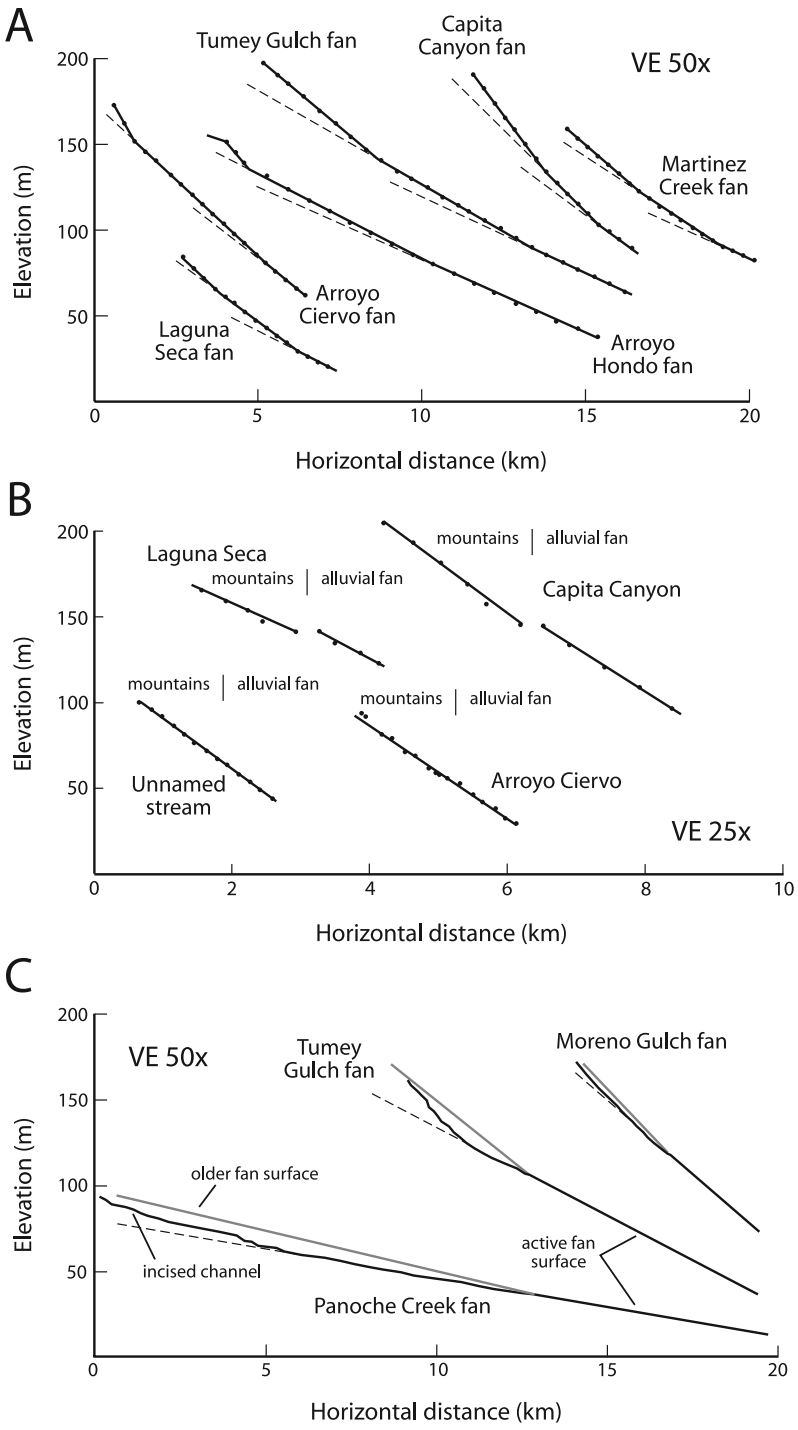

Figure 2. Fan radial profiles, modified from *Bull* [1964]. (a) Radial profiles of fan surfaces from fan head to toe. Dots are data points, and solid lines are linear segments interpolated by *Bull* [1964]. Thin dashed lines show the upslope continuation of segments. Profiles have been shifted horizontally and vertically for clarity. Vertical exaggeration is 50×. (b) Radial profiles of channels within catchments ("mountains") and adjacent, active fan surfaces ("alluvial fan"). Symbols are as in Figure 2a. Profiles have been shifted horizontally and vertically for clarity. Vertical exaggeration is 25×. (c) Radial profiles of older fan depositional segments (grey lines) and active channels (black lines) on fans with incised heads. Thin dashed lines show the upslope continuation of the active depositional segments. Profiles have been shifted horizontally and vertically for clarity. Vertical exaggeration is 50×.

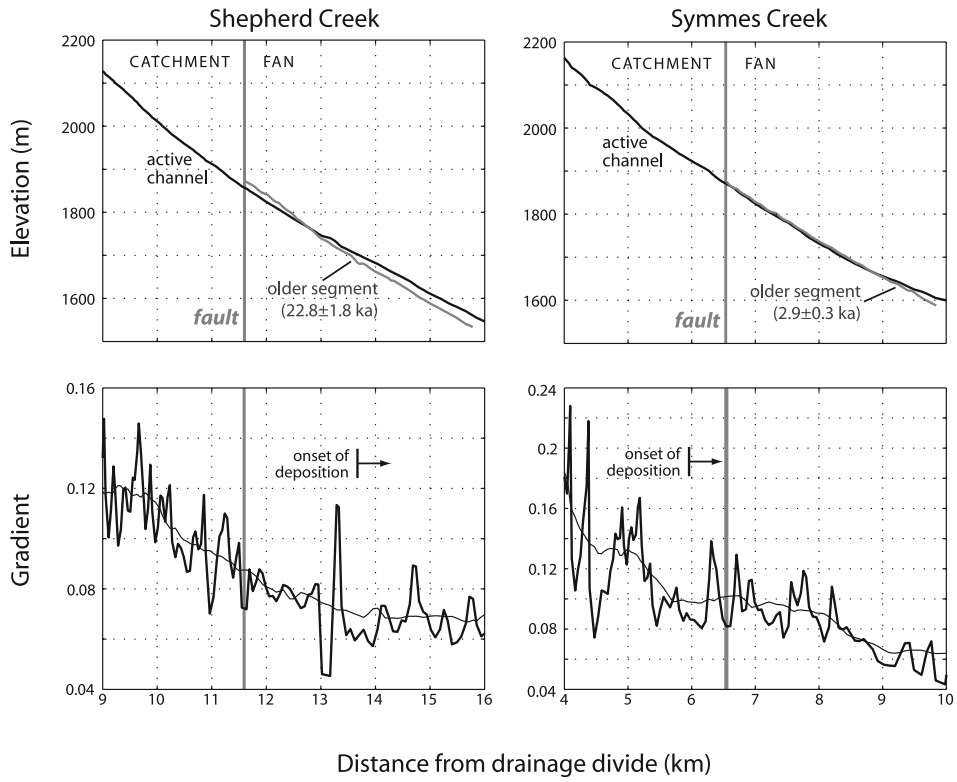

Figure 3. Profiles of active and abandoned channels on Shepherd Creek and Symmes Creek fans, Owens Valley, California. Thick vertical lines show the position of the active, normal slip Sierra Nevada frontal fault that separates catchments (to the left of fault) from fans (to the right). (top) Profiles of presently active channel in both catchment and fan (black lines), as well as profiles of older, inactive fan depositional segments (grey lines). Note that the channels are alluvial on both catchment and fan; bedrock exposure is limited to the upstream portions of both catchments. Ages of older segments are averages of 3–7 surface exposure ages derived from cosmogenic ^{10}Be analysis [*Dühnforth et al.*, 2007]. (bottom) Gradient of active channel in both catchment and fan, derived from a 10 m DTM (thick black lines), as well as 21-point smoothed curves (thin black line). Arrows mark the onset of significant fan deposition, which need not coincide with the position of the fault. The head of Shepherd Creek fan is incised, so the modern channel has a lower slope than the older fan segment, and fan deposition does not begin until about 2 km downstream of the fault. Symmes Creek fan is not incised, so the modern channel is coincident with the older segment and fan deposition occurs on both sides of the fault. On both fans, fan slope is approximately uniform for ~2 km beyond the onset of deposition.

head to toe. In contrast, high subsidence rates in the basin should lead to proximal deposition and thus small fans, with short radial lengths. At present, the shortage of data on catchment erosion rates, fan deposition rates, and fan volumes in well-constrained tectonic settings does not allow us to deconvolve these competing effects from those of catchment lithology and erodibility.

2.2. Fan Slopes and Radial Profiles

[9] Fan surface slope appears to vary systematically with catchment area and catchment lithology [e.g., *Bull*, 1964; *Denny*, 1965]. It is important to realize, however, that deposition rarely occurs over the entire fan surface at any one time [*Blair and McPherson*, 1998]. Instead, fans are commonly built of a number of depositional segments of different age [*Bull*, 1964; *Denny*, 1965]. *Bull* [1964] showed that the surface slopes of segments on many fans in California and Nevada are uniform, and that segment boundaries are marked by abrupt breaks in slope (Figure 2a). A number of authors have suggested, either explicitly or implicitly, that fan slope is a function of depositional process, with debris flow fans being systematically steeper than fluvial fans [e.g., *Blair and McPherson*, 1994; *Oguchi and Ohmori*, 1994; *Milana and Ruzycki*, 1999]. Such a simple relationship is somewhat complicated by the observations that (1) debris flow fans can exhibit a wide range of depositional slopes, down to ~0.5° in the case of lahar-dominated fans [*Hungr et al.*, 2005], and (2) individual fans are commonly formed by a range of processes, with fluvial sediment transport and granular debris flows being the endmembers of a broad process spectrum [*Saito and Oguchi*, 2005].

[10] *Bull* [1964] also showed that the slope of the active channel in the lowermost 1–2 km of the catchment is the same as the active depositional segment on the fan, and the radial profiles of older fan segments are often colinear with strath or fill terrace remnants in the lower catchment (Figures 2b and 2c). This important observation is not

limited to the fluvial San Joaquin Valley fans that were studied by *Bull* [1964]; debris flow fans in Owens Valley, California, show identical patterns of (1) linear fan segments that were active at different times and (2) colinearity between the lowermost 1–2 km of the catchment and the active depositional fan segment (Figure 3). Likewise, *Talling and Sowter* [1998] demonstrated general continuity of fan slope with channel slope across the mountain front of the Apennines, in central Italy. This continuity in both elevation and slope between catchment and fan, despite marked changes in channel confinement and substrate, is somewhat surprising. It suggests that (1) the catchment and fan form a linked longitudinal profile; (2) this profile is in equilibrium, or in a transient state toward equilibrium, with processes shaping the entire catchment fan system; and (3) ultimate base level for the catchment fan system is found at the fan toe (Figure 1).

[11] *Bull* [1964] used the colinearity of catchment and fan surfaces to argue that the generation of fan segments with different slopes is driven by changes in the balance of erosion and tectonics in the catchment, rather than by intrinsic processes on the fan. In his model, increasing fault slip rate creates higher slopes in the catchment and thus a steepening of the fan surface. If this dominance of rock uplift over erosion persists, it will generate a set of backstepping fan segments, with ever steeper segment slopes and smaller radial lengths. Conversely, long-term dominance of erosion over rock uplift should yield shallower catchment gradients through time, lower fan slopes, and a downward-stepping set of fan segments.

2.3. Summary of Observations

[12] These observations provide us with a set of geometrical and geomorphic constraints that must be satisfied by any model of a catchment fan system. Besides the overall form of the catchment fan pair (i.e., a generally concave-up catchment channel, and a wedge-shaped fan), these include (1) fan radial length that varies as some function of fault slip rate and sediment supply; (2) approximately uniform radial slopes on the active fan surface; (3) slope and elevation continuity between the lowermost catchment and the active fan surface; (4) the potential for segmentation into different depositional lobes; and (5) both basinward and rangeward stepping of the active fan toe.

3. A One-Dimensional Coupled Catchment Fan Model

[13] It is clear from the summary above that a number of different agents have been invoked to explain fan geometry, and in particular changes in fan surface form. We thus develop a simple numerical model of a catchment fan system, to see whether these agents, changes in fault slip rate, changes in climatic variables, lithological effects, and autocyclic ''tintinnabulations'' [*Humphrey and Heller*, 1995], produce distinct topographic or stratigraphic fingerprints that can be sought in the geological record. The goal of our numerical modeling is to explore the first-order relationships and feedbacks between rock uplift, erosion and deposition in a catchment fan system, rather than to reproduce detailed patterns of channel fan dynamics such as transient incision or stratigraphic stacking.

3.1. Catchment Erosion

[14] The basis for the catchment portion of the model is conservation of mass in one dimension:

$$\frac{\partial z}{\partial t} = U(x,t) - \frac{\partial q_s}{\partial x} \tag{2}$$

where x is downstream distance (m), z is the elevation of the surface (m), $U(x, t)$ is the rock uplift rate as a function of time and space (m yr^{-1}), and q_s is the total sediment discharge per unit width (m^2 yr^{-1}). We assume a simple transport-limited flux law that combines dispersive and concentrative terms [e.g., *Smith and Bretherton*, 1972; *Simpson and Schlunegger*, 2003]:

$$q_s = -\left(\kappa\frac{\partial z}{\partial x} + c_t(\alpha x)^m\frac{\partial z}{\partial x}\right) \tag{3}$$

where $\partial z/\partial x$ is the local slope (dimensionless), α is precipitation rate (m yr^{-1}), κ is a linear diffusivity (m^2 yr^{-1}), c_t is a nonlinear transport coefficient ((m^2 yr^{-1})$^{1-m}$), and m is a dimensionless exponent. Precipitation rate α is assumed to be uniform throughout the catchment, so that the quantity αx yields the water discharge per unit width. Note that we implicitly assume a slope exponent of 1, consistent with a system that is dominated by gravel bedload transport [*Howard*, 1980; *Whipple and Tucker*, 2002]. We use equation (3) because it is the simplest general expression that allows for the simultaneous development of both a diffusive hillslope and incisive channel, depending on the value of x [*Simpson and Schlunegger*, 2003]. Such a transport-limited flux law is likely to be most appropriate in orogens underlain by weak lithologies [*Talling*, 2000; *Whipple and Tucker*, 2002], or where the catchment channel is at least partly sediment mantled (Figure 3). A detachment-limited relationship would yield a similar steady-state catchment form and long-term sediment efflux, but would differ in the detailed, transient response to perturbations [e.g., *Whipple and Tucker*, 2002; *Tucker and Whipple*, 2002; *Whipple*, 2004]. As we are primarily interested in the overall form of the catchment fan system, we take advantage of the simplicity and ease of implementation of equation (3).

[15] Combining equations (2)–(3) yields an expression for the rate of surface change with time:

$$\frac{\partial z}{\partial t} = U(x,t) + \frac{\partial}{\partial x}\left(\left[\kappa + c_t(\alpha x)^m\right]\frac{\partial z}{\partial x}\right) \tag{4}$$

Note that the term in square brackets can be thought of as a system diffusivity, with units of m^2 yr^{-1}. It consists of a linear or ''hillslope'' diffusivity κ, and a nonlinear or ''fluvial'' diffusivity that depends on precipitation rate α and downstream distance x.

3.2. Fan Deposition

[16] The observations that fan slope is (1) approximately uniform on a given depositional segment and (2) equal to the channel slope in the lowermost catchment (Figures 2 and 3) suggest that fan slope is largely a geometrical function of the balance between sediment supply and basin

accommodation and may be somewhat independent of the actual process of sediment delivery, provided there is minimal reworking on the fan. For a given basin geometry, the fan slope sets the length of the fan from head to toe, and thus dictates the volume of sediment in the basin; a high fan slope yields a short, relatively low volume fan. At the same time, because the fan slope is observed to be continuous with the channel slope at the catchment outlet, the fan slope also sets an important base level boundary condition on the catchment. A high fan slope at the channel fan boundary, and thus a steep catchment channel, promotes high erosion rates and a large sediment efflux. Conversely, a low fan slope, for example due to widespread aggradation on the fan surface, will lead to a low catchment channel slope and thus a small sediment efflux.

[17] To capture this dynamic linkage, we model the fan surface as a straight, sloping line from the catchment mouth. The toe of the fan occurs where this line intersects the predepositional topography, so that the toe position is controlled by the fan slope and the spatial pattern of basin subsidence. The channel slope at the catchment outlet is assumed to be equal to the fan slope, which is initially unknown. We iterate to find the value of fan slope that balances the volume of material eroded from the catchment with the volume of the fan. Increasing the fan slope increases the volume of material eroded but decreases the potential fan volume, and vice versa.

[18] Note that we strive to keep the model as simple as possible, in order to better understand the first-order responses of the system to tectonic or climatic perturbations. Our model differs from that of *Humphrey and Heller* [1995] in that (1) we assume a transport limited, rather than detachment limited, catchment; (2) the rock uplift pattern is spatially variable; (3) fan deposition is not assumed to be diffusional, but is based strictly on mass balance considerations and geometric observations; and (4) the slope of the fan, as well as the elevation of the fan head, acts as a lower base level condition on the catchment. Our fan model does not simulate a particular depositional process, such as streamflow or debris flow transport, but is driven strictly by mass balance considerations and the observed geometrical constraints on fan and catchment slopes. Because we consider only a one-dimensional system, we ignore variations in channel width, which may be important in allowing fan head incision and entrenchment [*Bull*, 1964; *Hooke*, 1967]. We also do not account for grain-size effects on fan geometry [e.g., *Paola et al.*, 1992; *Marr et al.*, 2000].

3.3. Experimental Design

[19] Model experiments are performed on a regularly spaced one-dimensional vector of x positions. For simplicity, we refer to the uplifting mountain block as the "footwall" and the subsiding basin as the "hanging wall" (Figure 1), although in the model the "fault" separating them is vertical. The footwall is 10 km long, while the hanging wall is 30 km long and is assumed to end in a playa or similarly low relief, low gradient basin floor (Figure 1). We simulate tectonic flux of material by imposing vertical displacements $U(x, t)$ that decay exponentially with distance from the fault (Figure 4). The decay length scale is 7500 m, which yields a comparable coseismic displacement profile to those observed in large normal fault earthquakes [e.g., *Stein and Barrientos*, 1985].

[20] We solve equation (4) within the footwall using the Galerkin finite element method with linear shape and weighting functions and nonlinear iterations [*Zienkiewicz and Taylor*, 2000]. The time derivative in equation (4) is discretized using an implicit finite difference scheme. This solution shapes the channel profile in the footwall block and determines the sediment flux to the hanging wall. The fan slope and channel slope at the catchment outlet are equal and are initially set to an arbitrary value. During each time step, the model iterates to find the fan slope that balances the volume of eroded sediment with the volume of the hanging wall fan. A no-flux boundary condition is imposed at the upstream end of the footwall.

[21] Details of the dimensions and parameters used in the experiments are given in Table 1. Each experiment begins with a horizontal initial topography, and is run for 5 Myr with constant tectonic and climatic conditions (Figure 4). We then perturb the resulting base run by imposing a step change in either the fault slip rate or the precipitation rate. All other parameters are left constant, allowing us to isolate the responses and associated timescales of both catchment and fan.

4. Results

4.1. Base Run

[22] At the end of the 5 Myr base run, a concave-up channel on the footwall is paired with a sloping hanging wall fan (Figure 4). Total fault slip is 10 km, comparable to large faults in regions of continental extension [*Densmore et al.*, 2004]. The early growth of the system is characterized by surface uplift in the footwall, headward migration of the

Figure 4. Results of the base run after 5 Myr of model run time with constant fault slip rate (1 mm yr^{-1}) and precipitation rate (1 m yr^{-1}). (a) Catchment topography and fan stratigraphy. Model space is divided into uplifting "footwall" and subsiding "hanging wall" domains, separated by active dip-slip fault at x = 10 km. Fault displacement rate decreases exponentially away from the fault. Heavy black lines show bedrock surface (lower curve) and topographic surface (upper curve). Thin black lines show deformed stratigraphic timelines in the basin, recorded every 250 kyr. Note progradation of fan toe and pinch-out against bedrock surface. Dotted line shows fault displacement envelope. Total fault slip is 10 km and is divided evenly between footwall uplift and hanging wall subsidence; note that displacement envelope in hanging wall is coincident with bedrock surface beneath the basin. (b) Sediment flux q_s at the catchment outlet as a function of time during the 5 Myr run. Dashed line shows the value of the tectonic flux into the footwall q_t, which is 2.75 m^2 yr^{-1}. Note mismatch between q_s and q_t at the end of the run. (c) Fan surface slope as a function of time during the run. (d) Fan radial length as a function of time during the run; radial length is measured from the fault to the point where the fan pinches out against bedrock. (e) Chronostratigraphic diagram of the basin; grey area shows lateral extent of basin sedimentation as a function of time.

drainage divide toward the left-hand edge of the space, and progradation of a fan that steepens with time. The channel profile achieves a smooth, concave-up profile with a total relief from divide to catchment mouth of ~500 m. Both fan slope and sediment flux at the catchment outlet vary approximately exponentially with time and approach steady values after several million years, with a time constant τ (defined by fitting the flux curve with an expression of the form $[1 - \exp(-t/\tau)]$) of 550 kyr.

[23] Progradation of the fan toe results in progressive onlap onto the subsiding basement, and construction of a wedge-shaped fan deposit that thins away from the fault (Figure 4). While the progradation rate slows with time, it does not reach zero during the 5 Myr run. This somewhat surprising result is a consequence of the lack of topographic steady state in the base run. The sediment flux from the catchment q_s approaches a steady value by the end of the run, but this steady value is slightly greater than the constant

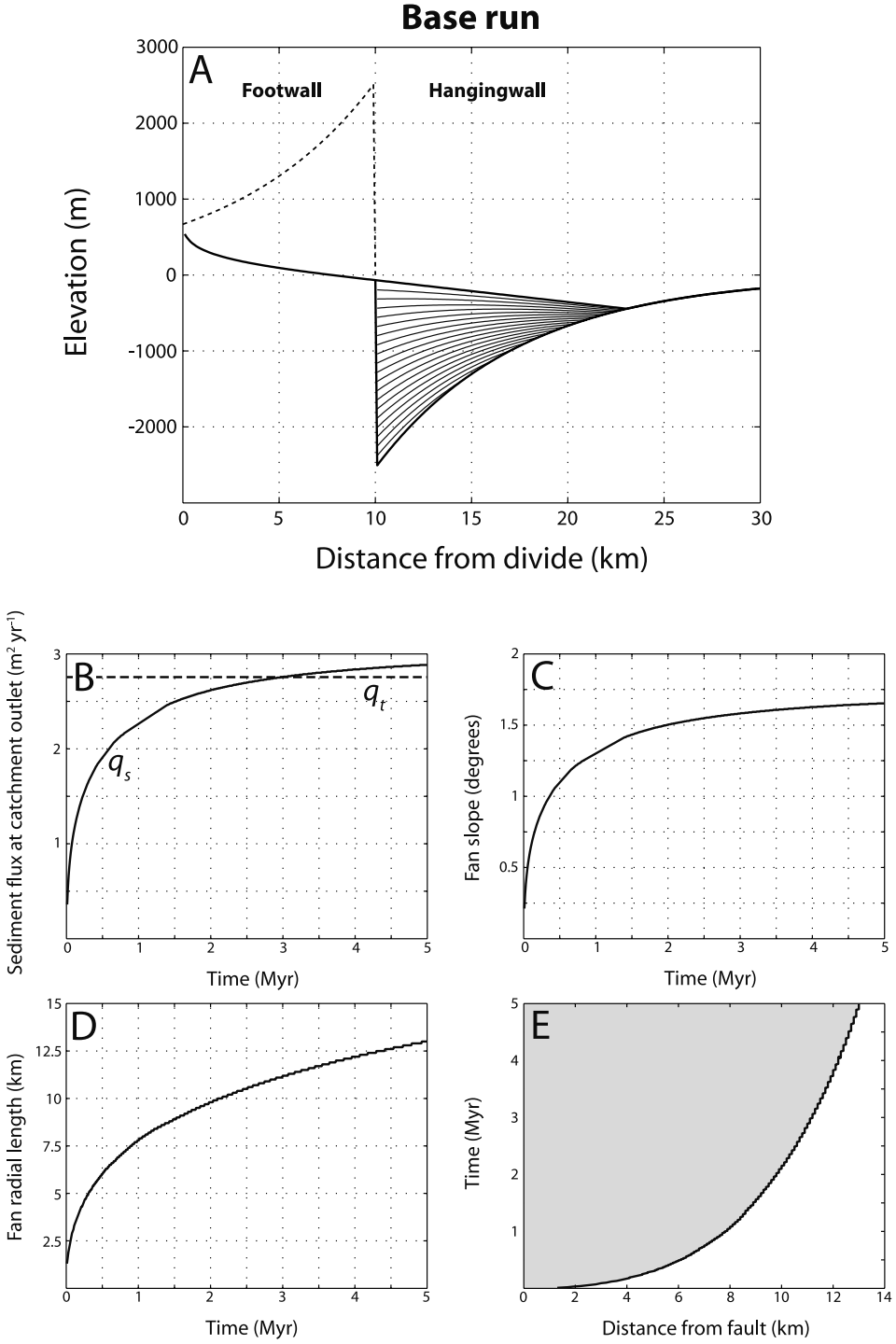

Figure 4

Table 1. Symbols and Model Parameters

Symbol	Name	Value and Units
A_c	catchment area	m^2
A_f	fan area	m^2
C	fan area coefficient	-
c_t	nonlinear sediment transport coefficient	1×10^{-6} $(m^2\ yr^{-1})^{1-m}$
dt	time step	1000 years
dx	cell size	100 m
L	footwall catchment length	10^4 m
m	slope exponent	2
n	fan area exponent	-
q_s	sediment flux	$m^2\ yr^{-1}$
q_t	tectonic flux	$m^2\ yr^{-1}$
t	run time	Y
U	rock uplift rate	$m\ yr^{-1}$
U_0	rock uplift rate at fault	1×10^{-3} m yr^{-1} in base run
x, z	horizontal and vertical position	M
α	precipitation rate	1 m yr^{-1} in base run
κ	linear diffusivity	0.01 $m^2\ yr^{-1}$
θ	dimensionless fan slope parameter	-
τ	time constant	years

tectonic flux into the footwall $q_t = \langle U \rangle L$, where $\langle U \rangle$ is the mean rock uplift rate and L is the length of the footwall catchment (Figure 4). The result of this imbalance is that the catchment achieves a steady form and relief, but this form translates downward because of net removal of mass from the footwall. When combined with the spatially variable (but nonzero) hanging wall subsidence rate, this leads to a slowly prograding fan toe. These results highlight the often unappreciated fact that, for a landscape at "equilibrium", the time derivative in equation (4) need not be zero, and that neither flux steady state ($q_s = q_t$) nor topographic steady state ($\partial z/\partial t = 0$; *Willett and Brandon* [2002]) are necessary to achieve steady catchment relief.

4.2. Slip Rate Perturbations

[24] To evaluate the response of the base run to tectonic perturbations, we vary the slip rate by a factor of 2 after 5 Myr of model run time, and run the model for an additional 5 Myr. Doubling the slip rate from 1 to 2 mm yr^{-1} results in an increase in fan slope and sediment flux at the catchment mouth (Figure 5). Both parameters approach new equilibrium values with a time constant of 630 kyr, approximately equal to the response time during initial system growth. The increase in slip rate causes an instantaneous increase in the rate of accommodation generation, which in turn causes an initial back-stepping of the fan toe by about 8 km [e.g., *Gordon and Heller*, 1993; *Allen and Densmore*, 2000]. As the sediment flux from the catchment gradually increases in response to the higher slip rate, the fan toe progrades again and onlaps onto older fan deposits with an angular unconformity, eventually extending beyond the preperturbation fan limit (Figure 5). The total duration of this back-stepping prograding event, from the onset of the slip rate perturbation until the fan toe reaches its previous extent, is about 2.5 Myr. Note that the increased slip rate after the perturbation results in significantly higher sediment thickness and deposition rates compared to the preperturbation fan (Figure 5).

[25] When the slip rate is halved from 1 to 0.5 mm yr^{-1}, catchment flux and fan slope decay to lower equilibrium values, again with a time constant of approximately 500 kyr (Figure 6). The fan toe progrades rapidly at first because of the decreased rate of accommodation generation, but then slows and reaches a fixed location as sediment supply decays. This progradation, combined with the simultaneous decrease in fan slope, produces a distinctive sheet-like stratigraphic unit that maintains a nearly uniform thickness across the entire fan surface (Figure 6). Note that there is no change in the pattern of tectonic accommodation generation during deposition of this distinct unit, and subsequent depositional units revert to a more usual wedge shape that thins away from the fault. The decrease in the rate of accommodation generation means that postperturbation sedimentary units are thinner, and deposition rates are lower, than before the change in slip rate.

4.3. Precipitation Rate Perturbations

[26] In the second set of experiments, we explore the response of the system to variations in precipitation rate. As before, we perturb the base run by varying the precipitation rate after 5 Myr, and then run the model for an additional 5 Myr. Increasing the precipitation rate by 50% (from 1 to 1.5 m yr^{-1}) causes the sediment flux from the catchment q_s to rise instantaneously, because the increase is felt simultaneously across the entire catchment (Figure 7). The flux then decays back to a new equilibrium level that is about 12% higher than the preperturbation value, with a time constant of 280 kyr. The new equilibrium flux is considerably higher than the input tectonic flux q_t, again emphasizing that a balance between q_s and q_t is not required to generate steady catchment relief, and demonstrating that the imbalance between q_s and q_t is at least partly dependent on the precipitation rate.

[27] As with a decrease in slip rate, increasing the precipitation rate leads to rapid progradation of the fan toe and deposition of a distinctive sheet-like sedimentary unit (Figure 7). Subsequent depositional units revert to a wedge shape that pinches out basinward. Note that, in this case, the thicknesses and deposition rates of preperturbation and postperturbation fan deposits are similar, because the rate of accommodation generation is unchanged throughout the experiment. This similarity in deposit thickness and the instantaneous increase in sediment flux are the only diagnostic observations that would allow us to differentiate an increase in precipitation rate from a comparable decrease in slip rate (e.g., compare Figures 6 and 7).

[28] Decreasing the precipitation rate by 50% (from 1 to 0.5 m yr^{-1}) produces a dramatic back-stepping of the fan toe, by more than 10 km (Figure 8). This back-stepping, and the associated increase of the fan slope, produces a significant angular unconformity. Subsequent deposition leads to renewed progradation of the fan toe, but the low precipitation rate and high fan slope means that the toe never reaches its former position. Catchment efflux drops instantaneously at the time of the perturbation and then recovers only slowly, with a time constant of 920 kyr. The fan slope rises rapidly at first, but the long time constant means that a new equilibrium slope is not reached by the end of the model run.

4.4. Controls on Fan Slope

[29] Clearly, both precipitation rate and fault slip rate are important controls on fan slope in our model. Precipitation

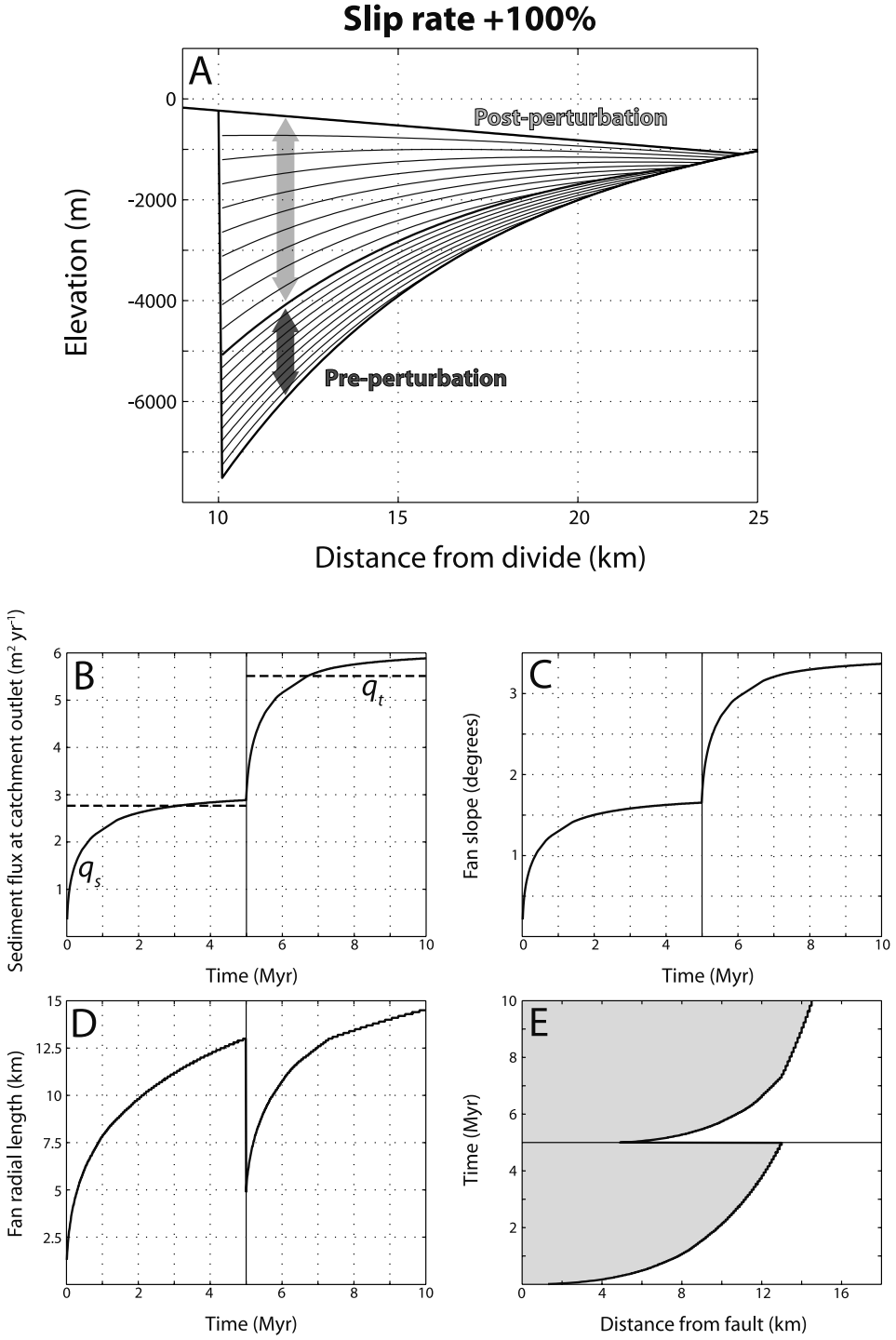

Figure 5. Experimental results following a doubled slip rate, to 2 mm yr^{-1}, after 5 Myr of model run time. Model behavior before the perturbation, from 0 to 5 Myr, is the same as in the base run (Figure 4). (a) Hanging wall stratigraphy before (dark grey arrow) and after (light grey arrow) the increase in slip rate. Deformed stratigraphic timelines are recorded every 500 kyr. Note increase in deposition rate and back-stepping prograding behavior of the fan toe, following the perturbation. (b) Sediment flux at the catchment outlet. Vertical line here and in subsequent panels marks the increase in slip rate at 5 Myr. Dashed line shows the tectonic flux into the footwall q_t. (c) Fan surface slope before and after the perturbation. (d) Fan radial length before and after the perturbation. Note back-stepping of the fan toe by about 8 km, followed by renewed progradation. (e) Chronostratigraphic diagram of the basin. Grey area shows lateral extent of basin sedimentation as a function of time. Solid horizontal line marks the increase in slip rate at 5 Myr.

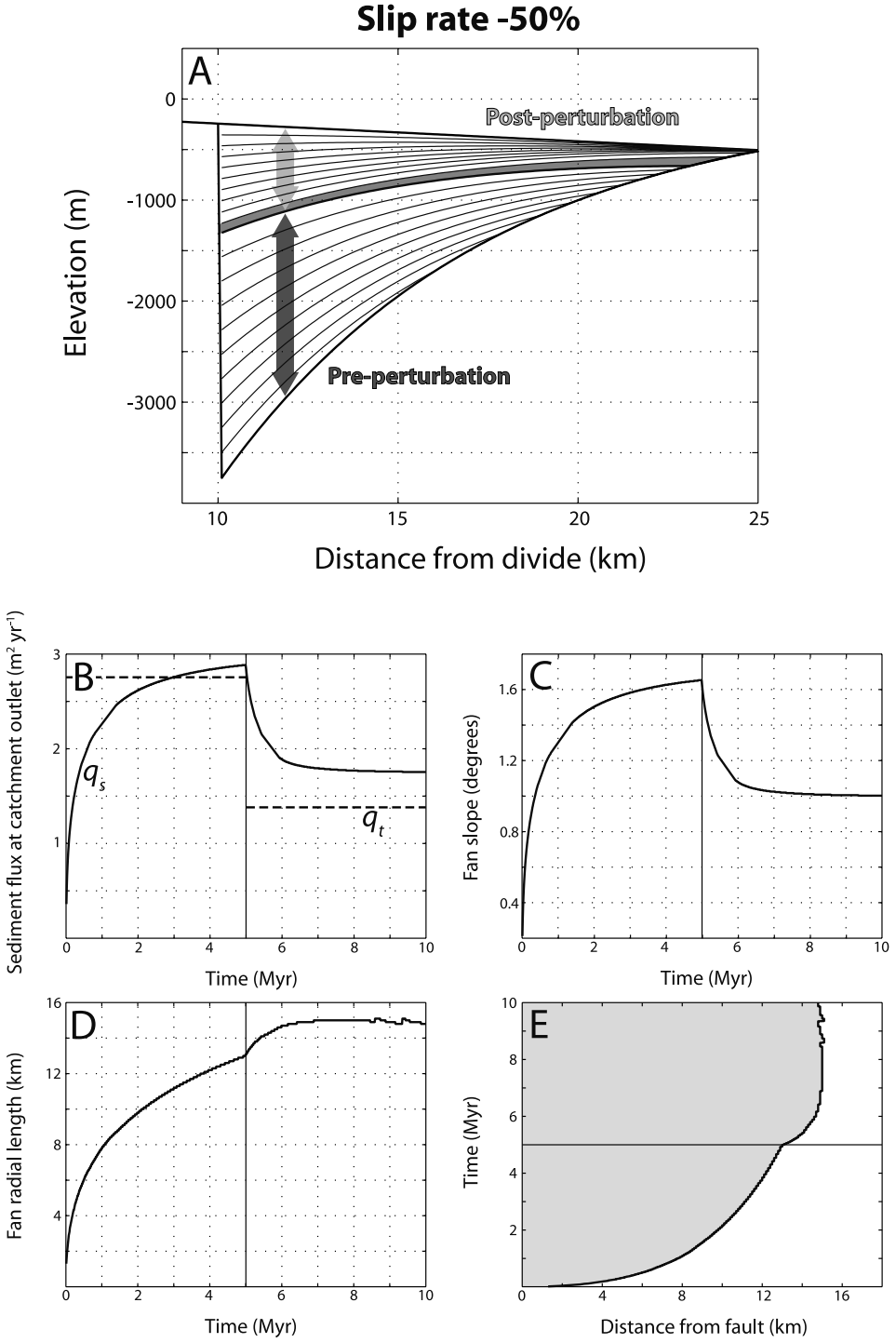

Figure 6. Experimental results following a halved slip rate, to 0.5 mm yr^{-1}, after 5 Myr of model run time. Model behavior before the perturbation, from 0 to 5 Myr, is the same as in the base run (Figure 4). (a) Hanging wall stratigraphy before (dark grey arrow) and after (light grey arrow) the increase in slip rate. Deformed stratigraphic time lines are recorded every 500 kyr. Note decrease in deposition rate and deposition of sheet-like unit (light grey) immediately after perturbation. Fan toe progrades, then stabilizes at an equilibrium position. (b) Sediment flux at the catchment outlet. Vertical line here and in subsequent panels marks the decrease in slip rate at 5 Myr. Dashed line shows the tectonic flux into the footwall q_t. (c) Fan surface slope before and after the perturbation. (d) Fan radial length before and after the perturbation. Note minor progradation of the fan toe, followed by stabilization. (e) Chronostratigraphic diagram of the basin. Grey area shows lateral extent of basin sedimentation as a function of time. Solid horizontal line marks the decrease in slip rate at 5 Myr.

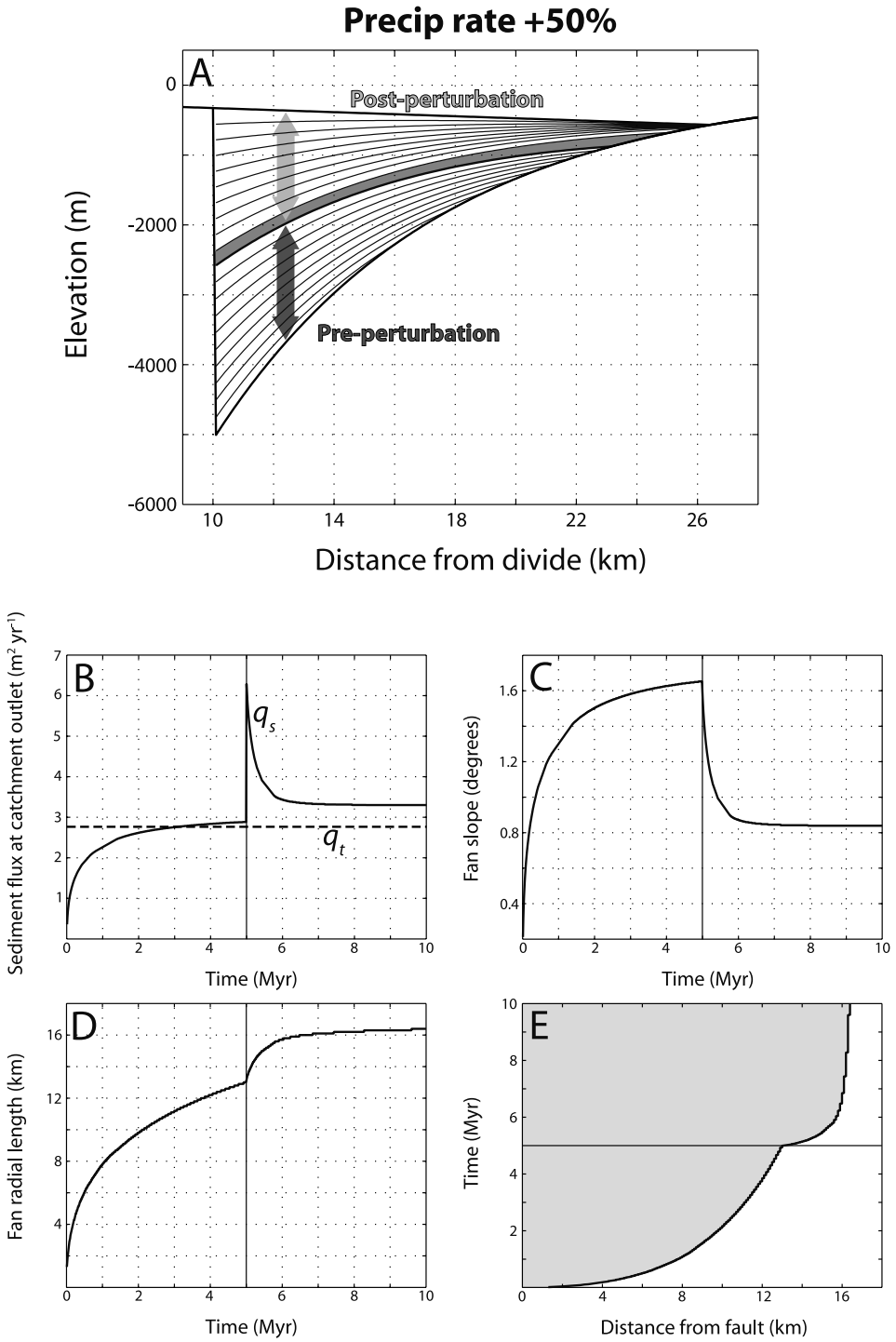

Figure 7. Experimental results following a 50% increase in the precipitation rate, to 1.5 m yr^{-1}, after 5 Myr of model run time. Model behavior before the perturbation, from 0 to 5 Myr, is the same as in the base run (Figure 4). (a) Hanging wall stratigraphy before (dark grey arrow) and after (light grey arrow) the increase in slip rate. Deformed stratigraphic time lines are recorded every 500 kyr. Fan deposition rate is unaffected by the perturbation. Increased precipitation rate leads to deposition of sheet-like unit (light grey) immediately after perturbation. Fan toe progrades, then stabilizes at an equilibrium position. (b) Sediment flux at the catchment outlet. Vertical line here and in subsequent panels marks the increase in precipitation rate at 5 Myr. Dashed line shows the tectonic flux into the footwall q_t, which remains constant during the run. (c) Fan surface slope before and after the perturbation. (d) Fan radial length before and after the perturbation. Note minor progradation of the fan toe, followed by stabilization. (e) Chronostratigraphic diagram of the basin. Grey area shows lateral extent of basin sedimentation as a function of time. Solid horizontal line marks the increase in precipitation rate at 5 Myr.

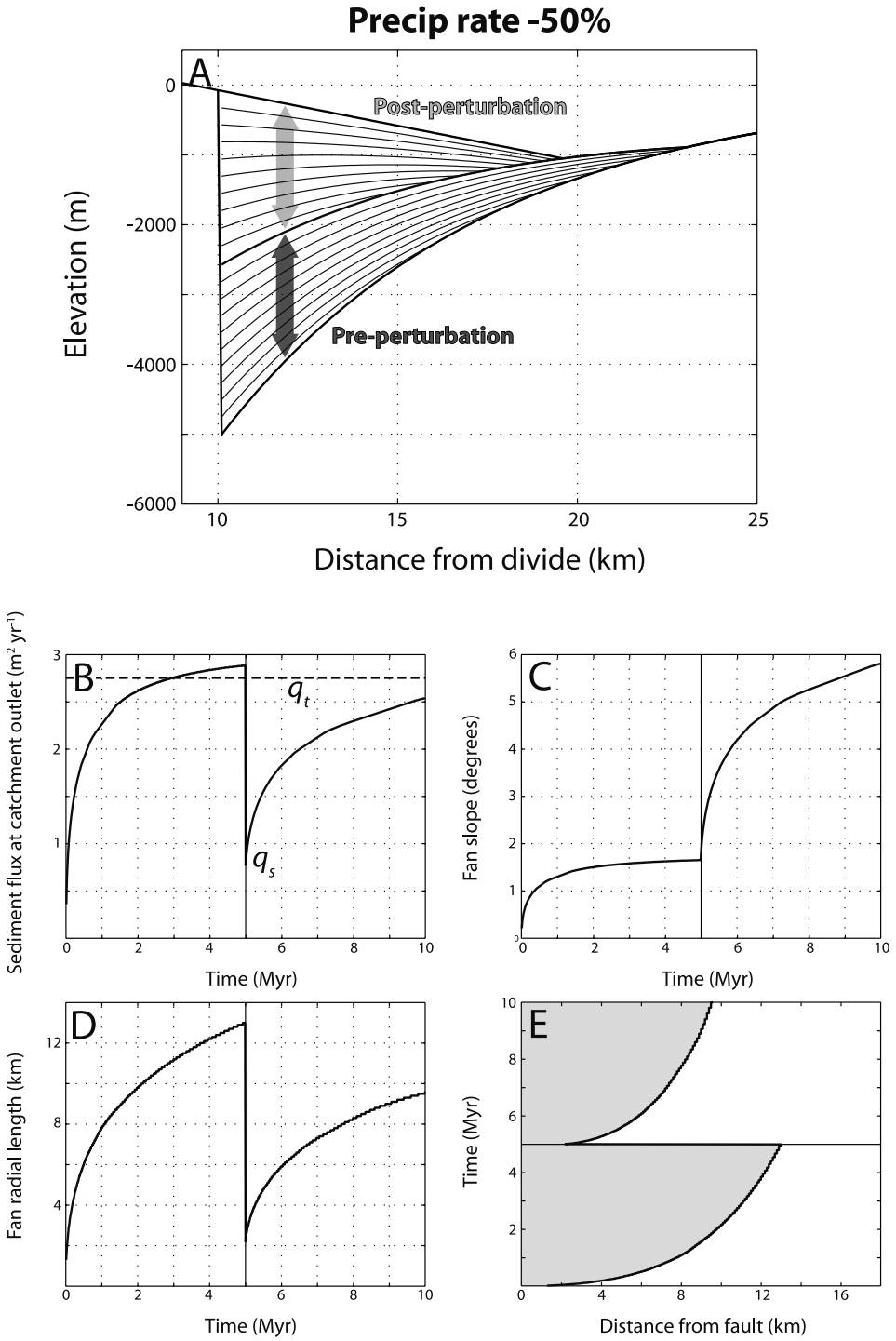

Figure 8. Experimental results following a 50% decrease in precipitation rate, to 0.5 m yr^{-1}, after 5 Myr of model run time. Model behavior before the perturbation, from 0 to 5 Myr, is the same as in the base run (Figure 4). (a) Hanging wall stratigraphy before (dark grey arrow) and after (light grey arrow) the decrease in precipitation rate. Deformed stratigraphic time lines are recorded every 500 kyr. Fan deposition rate is unaffected by the perturbation. Note back-stepping prograding behavior of fan toe and marked angular unconformity following the perturbation. (b) Sediment flux at the catchment outlet. Vertical line here and in subsequent panels marks the decrease in precipitation rate at 5 Myr. Dashed line shows the tectonic flux into the footwall q_t, which remains constant during the run. (c) Fan surface slope before and after the perturbation. (d) Fan radial length before and after the perturbation. Note back-stepping of the fan toe by more than 10 km, followed by renewed progradation. (e) Chronostratigraphic diagram of the basin. Grey area shows lateral extent of basin sedimentation as a function of time. Solid horizontal line marks the decrease in precipitation rate at 5 Myr.

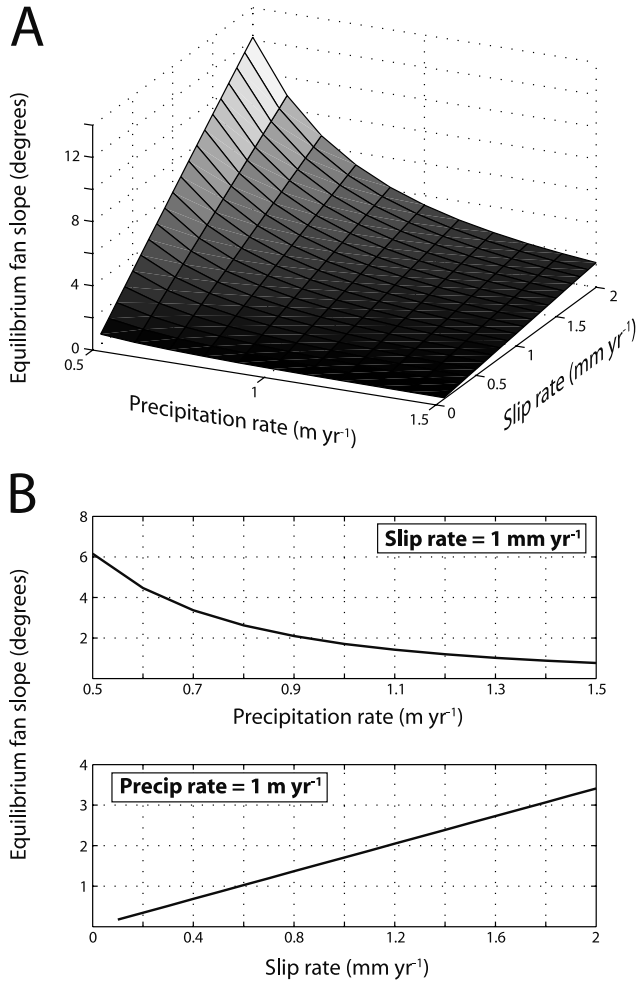

Figure 9. Controls on equilibrium fan slope. Model was run with different combinations of slip rate and precipitation rate until a constant fan slope was achieved. Precipitation rate was varied from 0.5 to 1.5 m yr^{-1} in 0.1 m yr^{-1} increments, while slip rate was varied from 0.1 to 2 mm yr^{-1} in 0.1 mm yr^{-1} increments. (a) Surface plot of fan slope as function of precipitation and slip rates. High fan slopes (>8–10°) are possible only at the lowest precipitation rates and highest slip rates. (b) Sections of the surface in Figure 9a showing functional dependence on precipitation and slip rates. (Figure 9b, top) Dependence on precipitation rate at a fixed slip rate of 1 mm yr^{-1}; (Figure 9b, bottom) Dependence on slip rate at a fixed precipitation rate of 1 m yr^{-1}.

rate determines sediment supply, while slip rate determines both sediment supply (through catchment gradient) and the amount of accommodation. To evaluate their relative influence on fan slope, we systematically vary both parameters and calculate the resulting steady state fan slope. Precipitation rate is varied from 0.5 to 1.5 m yr^{-1} in 0.1 m yr^{-1} increments, while slip rate is varied from 0.1 to 2 mm yr^{-1} in 0.1 mm yr^{-1} increments, both geologically reasonable ranges.

[30] The computed equilibrium fan slopes shows that fan slope depends linearly on slip rate, but varies as the inverse square of precipitation rate (Figure 9). Sensitivity to tectonics is lowest at high precipitation rates, because sediment fluxes are uniformly high and the basin is filled (i.e., fan slopes are low) regardless of slip rate. Conversely, sensitivity to climate is lowest at low slip rates, because little accommodation is generated and again the basin is always filled. Very steep (>8–10°) fans, such as those in the Black Mountains of Death Valley [*Denny*, 1965], can only form through a combination of very high slip rates and low precipitation rates.

[31] The simple relationships in Figure 9 suggest that a nondimensional form of equation (3) should yield an analytical expression for equilibrium fan slope. We introduce the following variable replacements:

$$\overline{x} = \frac{x}{L},\ \overline{z} = \frac{z}{L},\ \overline{t} = t\frac{U_0}{L},\ \overline{q}_s = q_s\frac{1}{LU_0} \tag{5}$$

where L is the length of the footwall catchment, U_0 is the slip rate at the fault, and the bars denote dimensionless variables. Substituting these into equation (3) yields

$$\overline{q}_s = -\left(\kappa\frac{1}{LU_0} + \frac{c_t\alpha^m L^m}{LU_0}\overline{x}^m\right)\frac{\partial\overline{z}}{\partial\overline{x}} \tag{6}$$

[32] The flux at the catchment outlet $\overline{q}_{sout}$ determines the equilibrium fan slope. At the outlet, $\overline{x} = 1$ and the first term in brackets is small compared with the second, so we can simplify equation (6) to

$$\frac{\partial\overline{z}}{\partial\overline{x}} = \frac{U_0}{c_t\alpha^m L^{m-1}}\overline{q}_{sout} \tag{7}$$

$$\frac{\partial\overline{z}}{\partial\overline{x}} = \theta\overline{q}_{sout} \tag{8}$$

where $\theta = U_0/(c_t\alpha^m L^{m-1})$. The dimensionless grouping of constants θ illustrates the relative role of climate and tectonics in setting fan slope in the model, and is somewhat analogous to the uplift erosion number proposed by *Whipple and Tucker* [1999]. For a given sediment flux from the catchment, equilibrium fan slope varies linearly with fault slip rate U_0, and varies inversely with lithology (parameterized by the transport coefficient c_t), precipitation rate α, and catchment length L. Thus equation (8) collapses the variability evident in Figure 9 into a single, quasi-linear relationship for fan slope (Figure 10).

4.5. System Response Times

[33] The strikingly different responses to increases or decreases in the precipitation rate suggest that, not surprisingly, the time required for the catchment fan system to reach a new equilibrium is dependent upon the system diffusivity (e.g., equation (4)). To further explore this dependence, we again systematically vary both precipitation rate and slip rate as in the previous experiment. We begin with horizontal initial topography, as in the base run experiment, and run the model with a specified slip rate and precipitation rate until equilibrium values of sediment flux and fan slope are reached. We assess the response time using the time constant τ of the flux curve, defined by

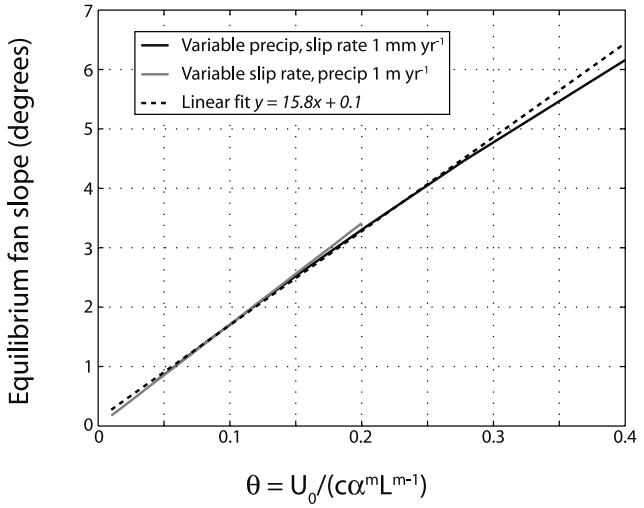

Figure 10. Equilibrium fan slope as a function of dimensionless parameter θ. Black line shows fan slope as a function of variable precipitation rate at a fixed slip rate of 1 mm yr^{-1}; compare with Figure 9b, top. Grey line shows fan slope as a function of variable slip rate, for a fixed precipitation rate of 1 m yr^{-1}; compare with Figure 9b, bottom. Dashed line is linear fit to both data sets. The dimensionless parameter θ collapses tectonic and climatic controls on fan slope into a single, quasi-linear relationship.

fitting an expression of the form $[1 - \exp(-t/\tau)]$. Perturbing the base run, rather than starting with a horizontal initial topography, yields similar results for the time constant for given values of slip and precipitation rates.

[34] As expected, the time constant decreases with increasing precipitation rate, and thus with increasing system diffusivity (Figure 11). Because equation (4) is a diffusion equation, the time constant varies approximately inversely with the system diffusivity, and thus as the inverse square of the precipitation rate. A more unexpected result is that the time constant is largely independent of the slip rate, for a reasonable range of values from 0.1 to 2 mm yr^{-1} (Figure 11). In other words, the response time of the model depends strongly on the system diffusivity, but not on the rate of rock uplift (which governs accommodation generation and base level change, and imposes a tectonically induced slope $\partial z/\partial x$ to the system).

5. Discussion and Conclusions

[35] Our model can be used to show that many aspects of sediment fan morphology can be explained in terms of perturbations to tectonic or climatic boundary conditions. An increase in fault slip rate, or a decrease in precipitation rate, leads to an increase in fan slope, and to back-stepping and subsequent progradation of the fan toe. These responses occur because the perturbations cause a temporary dominance of tectonic deformation over the ability of the sediment transport system to redistribute mass; in other words, the first term on the right in equation (4) overwhelms the second. Conversely, a decrease in slip rate, or an increase in precipitation rate, allows the sediment transport system to temporarily overcome the effects of rock uplift. This results in a decrease in fan slope, and to progradation and stabilization of the fan toe. Although tectonic and climatic perturbations may appear to have broadly similar effects on the fan morphology, there are two key differences: (1) fan deposition rates are largely independent of precipitation variations but strongly linked to changes in slip rate [e.g., *Whipple and Trayler*, 1996]; and (2) the sediment flux at the catchment outlet responds very rapidly to changes in precipitation rate but relatively slowly (over timescales of $\sim$0.5–2 Myr) to changes in slip rate.

[36] The long response times shown by the model, while partly a function of our choice of parameter values, underscore the difficulty of recording short-duration, high-frequency perturbations in large-scale fan morphology or stratigraphic architecture. Even a simple step-change increase in slip rate gives rise to a cycle of fan toe backstepping and progradation, with a significant angular unconformity between preperturbation and postperturbation stratigraphy, over a timescale of $\sim 10^5$ to 10^6 years. While the details of this transient response are partly dependent on the catchment sediment efflux (and thus on the chosen erosion rule), a general outcome of our model is that adjustment of kilometer-scale fan surface slope or toe position is simply too slow to faithfully reflect high-frequency variations in,

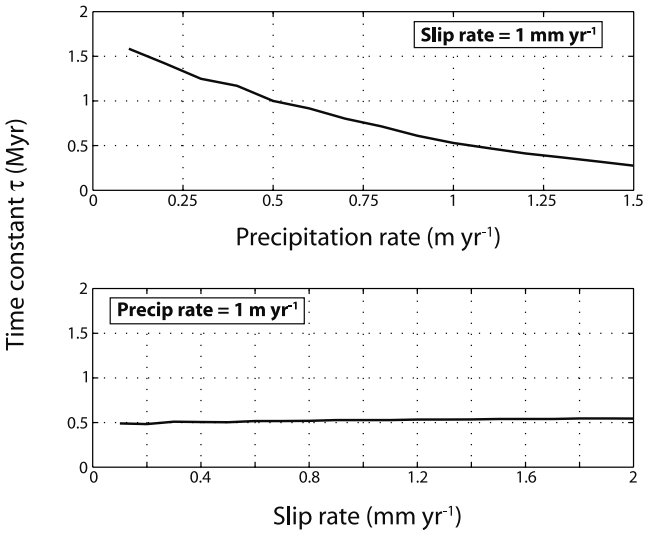

Figure 11. Response times as a function of precipitation rate (top) and slip rate (bottom). Model is run from a flat initial topography until a steady sediment flux at the catchment outlet is achieved, similar to the base run in Figure 4. Response time for achievement of this equilibrium is expressed as exponential time constant τ, defined by fitting the sediment flux curve with an expression of the form $[1 - \exp(-t/\tau)]$. Figure 11, top, shows time constant as a function of precipitation rate, which is varied from 0.1 to 1.5 m yr^{-1} in 0.1 m yr^{-1} increments, for a fixed slip rate. Note approximately quadratic decay of time constant with increasing precipitation rate, consistent with linear dependence of time constant on system diffusivity (equation (4)). Figure 11, bottom, shows time constant as function of slip rate, which is varied from 0.1 to 2 mm yr^{-1} in 0.1 mm yr^{-1} increments, for a fixed precipitation rate. Response time is insensitive to slip rate over this geologically reasonable range.

for example, precipitation or water discharge. We identify two possible mechanisms that might circumvent this sluggish response and allow preservation of a high-frequency record. First, segmentation of the fan, caused by abandonment and preservation of older depositional lobes [*Bull*, 1964; *Hooke*, 1967], will preserve the fan slope at the time of abandonment and potentially allow its interpretation as a function of climatic and tectonic conditions. This implies that we should particularly seek fans with incised heads, where older depositional surfaces are preserved in the proximal part of the fan (e.g., Figure 3). Second, proximity to base level may provide an alternate means of "freezing" the fan morphology rapidly after a perturbation event. For example, Pliocene Gilbert deltas in the Loreto Basin in Baja California appear to record short-duration ($\sim 10^4$ y) slip rate variations on the basin-bounding Loreto fault [*Dorsey et al.*, 1997; *Mortimer et al.*, 2005]. Such preservation is possible because the sediments were deposited in shoal water environments, at or just below sea level, as individual progradational units [*Mortimer et al.*, 2005]. In closed or isolated basins, as are common in many continental rift settings, such a high-resolution record of base level change is unlikely to be deposited or preserved.

[37] A unique aspect of our model is that fan slope is assumed to be uniform and is dictated solely by mass balance considerations between the flux of material removed from a catchment and the rate of accommodation generation in the adjacent basin. Similar elements were incorporated into a conceptual model of sedimentation in flexural foreland basins by *Heller et al.* [1988], who attributed alternating phases of proximal stacking of coarse-grained wedges and distal deposition of sediment sheets to tectonic activity and quiescence, respectively. Our approach differs from that of other fan models in that we do not adopt a diffusive rule for sediment transport and deposition on the fan [e.g., *Paola et al.*, 1992; *Humphrey and Heller*, 1995; *Parker et al.*, 1998; *Marr et al.*, 2000]. Diffusive fan models with uniform diffusivity tend to produce concave-up surface profiles [e.g., *Marr et al.*, 2000; *Sun et al.*, 2002]. The near-uniformity of segment slopes on many natural fans suggests that diffusive fan transport models may be inappropriate in those settings unless diffusivity is somehow varied down-fan, perhaps associated with changes in grain size [*Blair and McPherson*, 1998; *Marr et al.*, 2000; *Stock et al.*, 2004] or channel width.

[38] By linking fan slope directly to catchment sediment flux, we are implicitly assuming that fan slope is inversely dependent on the "efficiency" of the sediment transport system in moving material out into the basin. A highly efficient system, driven for example by high water discharge, would generate high sediment discharge at the catchment mouth, necessitating a large fan with a low surface slope [*Oguchi and Ohmori*, 1994; *Milana and Ruzycki*, 1999]. This may be a better explanation for variations in fan surface slope than the simple process-based division between debris flow and alluvial fans outlined in section 2.2. A better way to address this would be to apply more realistic sediment transport algorithms to the fan surface; this is relatively straightforward in the case of streamflow-dominated fans [*Parker et al.*, 1998; *Marr et al.*, 2000; *Sun et al.*, 2002], but to our knowledge has not been attempted in the case of debris flow fans.

[39] **Acknowledgments.** Support for this research was provided by grants from the Swiss National Science Foundation (grants 2100-067624 and 200020-105225/1) and the U.S. National Science Foundation (grant EAR0207569). We thank Sébastien Castelltort, Patience Cowie, Andrea Cozzi, Nancye Dawers, Max Densmore, Miriam Dühnforth, Sanjeev Gupta, and Kelin Whipple for ideas and stimulating discussions. Constructive reviews by Sanjeev Gupta, Paul Heller, and an anonymous reviewer helped to clarify and focus the manuscript.

References

Allen, P. A. (2005), Striking a chord, *Nature*, *434*, 961.

Allen, P. A. (2007), Time scales of tectonic landscapes and their sediment routing systems, in *Earth's Dynamic Surface: Catastrophe and Continuity in Landscape Evolution*, Geol. Soc. of London Spec. Publ., in press.

Allen, P. A., and A. L. Densmore (2000), Sediment flux from an uplifting fault block, *Basin Res.*, *12*, 367–380.

Allen, P. A., and N. Hovius (1998), Sediment supply from landslide-dominated catchments: Implications for basin-margin fans, *Basin Res.*, *10*, 19–35.

Blair, T. C. (1999a), Sedimentary processes and facies of the waterlaid Anvil Spring Canyon alluvial fan, Death Valley, California, *Sedimentology*, *46*, 913–940.

Blair, T. C. (1999b), Sedimentology of the debris flow-dominated Warm Spring Canyon alluvial fan, Death Valley, California, *Sedimentology*, *46*, 941–965.

Blair, T. C., and J. G. McPherson (1994), Alluvial fan processes and forms, in *Geomorphology of Desert Environments*, edited by A. D. Abrahams and A. J. Parsons, pp. 354–402, CRC Press, Boca Raton, Fla.

Blair, T. C., and J. G. McPherson (1998), Recent debris-flow processes and resultant form and facies of the Dolomite alluvial fan, Owens Valley, California, *J. Sediment. Res.*, *68*, 800–818.

Bull, W. B. (1962), Relations of alluvial fan size and slope to drainage basin size and lithology in western Fresno County, California, *Prof. Pap., 450-B*, pp. 51–53, U.S. Geol. Surv., Washington D.C.

Bull, W. B. (1964), Geomorphology of segmented alluvial fans in western Fresno County, California, *Prof. Pap., 352-E*, 129 pp., U.S. Geol. Surv., Washington D.C.

Carretier, S., and F. Lucazeau (2005), How does alluvial sedimentation at range fronts modify the erosional dynamics of mountain catchments?, *Basin Res.*, *17*, 361–382.

Castelltort, S., and J. van den Driessche (2003), How plausible are high-frequency sediment supply-driven cycles in the stratigraphic record?, *Sediment. Geol.*, *157*, doi:10.1016/S0037-0738(03)00066-6.

Dade, W. B., and P. F. Friend (1998), Grain size, sediment transport regime, and channel slope in alluvial rivers, *J. Geol.*, *106*, 661–675.

Denny, C. S. (1965), Alluvial fans in the Death Valley region, California and Nevada, *Prof. Pap., 466*, 62 pp., U.S. Geol. Surv., Washington D.C.

Densmore, A. L., N. H. Dawers, S. Gupta, R. Guidon, and T. Goldin (2004), Footwall topographic development during continental extension, *J. Geophys. Res.*, *109*, F03001, doi:10.1029/2003JF000115.

Dorsey, R. J., P. J. Umhoefer, and P. D. Falk (1997), Earthquake clustering inferred from Pliocene Gilbert-type fan deltas in the Loreto basin, Baja California Sur, Mexico, *Geology*, *25*, 679–682.

Dühnforth, M., A. L. Densmore, S. Ivy-Ochs, and P. A. Allen (2007), Timing of debris-flow fan aggradation and incision on Shepherd and Symmes Creek fans, Owens Valley, California, deduced from cosmogenic ^{10}Be, *J. Geophys. Res.*, doi:10.1029/2006JF000562, in press.

Fernandes, N. F., and W. E. Dietrich (1997), Hillslope evolution by diffusive processes: The timescale for equilibrium adjustments, *Water Resour. Res.*, *33*, 1307–1318.

Fraser, G. S., and P. G. DeCelles (1992), Geomorphic controls on sediment accumulation at margins of foreland basins, *Basin Res.*, *4*, 233–252.

Gordon, I., and P. L. Heller (1993), Evaluating major controls on basin stratigraphy, Pine Valley, Nevada: Implications for syntectonic deposition, *Geol. Soc. Am. Bull.*, *105*, 47–55.

Heller, P. L., C. L. Angevine, N. S. Winslow, and C. Paola (1988), Two-phase stratigraphic model of foreland-basin sequences, *Geology*, *16*, 501–504.

Hooke, R. L. (1967), Processes on arid-region alluvial fans, *J. Geol.*, *75*, 438–460.

Hooke, R. L. (1968), Steady-state relationships on arid-region alluvial fans in closed basins, *Am. J. Sci.*, *266*, 609–629.

Hooke, R. L., and W. L. Rohrer (1977), Relative erodibility of source-area rock types, as determined from second-order variations in alluvial fan size, *Geol. Soc. Am. Bull.*, *88*, 1177–1182.

Howard, A. D. (1980), Thresholds in river regimes, in *Thresholds in Geomorphology*, edited by D. R. Coates and J. D. Vitek, pp. 227–258, Allen and Unwin, St. Leonards, N.S.W., Australia.

Humphrey, N., and P. L. Heller (1995), Natural oscillations in coupled geomorphic systems: An alternative origin for cyclic sedimentation, *Geology*, *23*, 499–502.

Hungr, O., S. McDougall, and M. Bovis (2005), Entrainment of material by debris flows, in *Debris-flow Hazards and Related Phenomena*, edited by M. Jakob and O. Hungr, pp. 135–158, Springer, New York.

Marr, J. G., J. B. Swenson, C. Paola, and V. R. Voller (2000), A two-diffusion model of fluvial stratigraphy in closed depositional basins, *Basin Res.*, *12*, 381–398.

Métivier, F., and Y. Gaudemer (1999), Stability of output fluxes of large rivers in South and East Asia during the last 2 million years: Implications for floodplain processes, *Basin Res.*, *11*, 293–303.

Métivier, F., Y. Gaudemer, P. Tapponier, and M. Klein (1999), Mass accumulation rates in Asia during the Cenozoic, *Geophys. J. Int.*, *137*, 280–318.

Milana, J. P., and L. Ruzycki (1999), Alluvial-fan slope as a function of sediment transport efficiency, *J. Sediment. Res.*, *69*, 553–562.

Mortimer, E., S. Gupta, and P. Cowie (2005), Nucleation and growth in coarse-grained deltas, Loreto Basin, Baja California Sur, Mexico: A response to episodic accelerations in fault displacement, *Basin Res.*, *17*, 337–359.

Oguchi, T., and H. Ohmori (1994), Analysis of relationships among alluvial fan area, source basin area, basin slope, and sediment yield, *Z. Geomorphol.*, *38*, 405–420.

Paola, C., P. L. Heller, and C. L. Angevine (1992), The large-scale dynamics of grain size variation in alluvial basins: 1, Theory, *Basin Res.*, *4*, 73–90.

Parker, G., C. Paola, K. X. Whipple, and D. Mohrig (1998), Alluvial fans formed by channelized fluvial and sheet flow: 1, Theory, *J. Hydraul. Eng.*, *24*, 985–995.

Pelletier, J. D. (2004), The influence of piedmont deposition on the time scale of mountain belt denudation, *Geophys. Res. Lett.*, *31*, L15502, doi:10.1029/2004GL020052.

Saito, K., and T. Oguchi (2005), Slope of alluvial fans in humid regions of Japan, Taiwan, and the Philippines, *Geomorphology*, *70*, 147–162.

Simpson, G., and F. Schlunegger (2003), Topographic evolution and morphology of surfaces evolving in response to coupled fluvial and hillslope sediment transport, *J. Geophys. Res.*, *108*(B6), 2300, doi:10.1029/2002JB002162.

Smith, T. R., and F. P. Bretherton (1972), Stability and the conservation of mass in drainage basin evolution, *Water Resour. Res.*, *8*, 1506–1529.

Snyder, N. P., K. X. Whipple, G. E. Tucker, and D. J. Merritts (2000), Landscape response to tectonic forcing: Digital elevation model analysis of stream profiles in the Mendocino triple junction region, Northern California, *Bull. Geol. Soc. Am.*, *112*, 1250–1263.

Stein, R. S., and S. E. Barrientos (1985), Planar high-angle faulting in the Basin and Range: geodetic analysis of the 1983 Borah Peak, Idaho, earthquake, *J. Geophys. Res.*, *90*, 11,355–11,366.

Stock, J. D., K. M. Schmidt, and D. M. Miller (2004), Observations on alluvial fans with relevance to recent sediment transport, *Eos Trans. AGU*, *85*(47), Fall Meet. Suppl., Abstract H41G-03.

Sun, T., C. Paola, G. Parker, and P. Meakin (2002), Fluvial fan deltas: Linking channel processes with large-scale morphodynamics, *Water Resour. Res.*, *38*(9), 1151, doi:10.1029/2001WR000284.

Talling, P. J. (2000), Self-organization of river networks to threshold states, *Water Resour. Res.*, *36*, 1119–1128.

Talling, P. J., and M. J. Sowter (1998), Erosion, deposition, and basin-wide variations in stream power and bed shear stress, *Basin Res.*, *10*, 87–108.

Tucker, G. E., and K. X. Whipple (2002), Topographic outcomes predicted by stream erosion models: sensitivity analysis and intermodel comparison, *J. Geophys. Res.*, *107*(B9), 2179, doi:10.1029/2001JB000162.

van der Beek, P., and P. Bishop (2003), Cenozoic river profile development in the upper Lachlan catchment (SE Australia) as a test of quantitative fluvial incision models, *J. Geophys. Res.*, *108*(B6), 2309, doi:10.1029/2002JB002125.

Whipple, K. X. (2001), Fluvial landscape response time: how plausible is steady-state denudation?, *Am. J. Sci.*, *301*, 313–325.

Whipple, K. X. (2004), Bedrock rivers and the geomorphology of active orogens, *Annu. Rev. Earth Planet. Sci.*, *32*, 151–185.

Whipple, K. X., and T. Dunne (1992), The influence of debris-flow rheology on fan morphology, Owens Valley, California, *Bull. Geol. Soc. Am.*, *104*, 887–900.

Whipple, K. X., and C. R. Trayler (1996), Tectonic control of fan size: The importance of spatially variable subsidence rates, *Basin Res.*, *8*, 351–366.

Whipple, K. X., and G. E. Tucker (1999), Dynamics of the stream power incision model: Implications for height limits of mountain ranges, landscape response time scales, and research needs, *J. Geophys. Res.*, *104*, 17,661–17,674.

Whipple, K. X., and G. E. Tucker (2002), Implications of sediment-flux-dependent river incision models for landscape evolution, *J. Geophys. Res.*, *107*(B2), 2039, doi:10.1029/2000JB000044.

Willett, S. D., and M. T. Brandon (2002), On steady states in mountain belts, *Geology*, *30*, 175–178.

Wobus, C., K. Whipple, E. Kirby, N. Snyder, J. Johnson, K. Spyropolou, B. T. Crosby, and D. Sheehan (2006), Tectonics from topography: Procedures, promise, and pitfalls, in *Tectonics, Climate, and Landscape Evolution*, *Geol. Soc. Am. Spec. Pap., 398*, edited by S. D. Willett et al., pp. 55–74, Geol. Soc. of Am., Boulder, CO.

Zienkiewicz, O. C., and R. L. Taylor (2000), *The Finite Element Method: Volume 1, The Basis*, 689 pp., Elsevier, New York.

P. A. Allen, Department of Earth Science and Engineering, Imperial College London, South Kensington Campus, London SW7 2AZ, UK.

A. L. Densmore and G. Simpson, Institute of Geology, Department of Earth Sciences, ETH Zürich, CH-8092 Zürich, Switzerland. (densmore@erdw.ethz.ch)